Electrochemical exfoliation of Ti_3AlC_2 MAX phase and Al^{3+} ion electrochemistry in aqueous electrolyte

5.1 Introduction

Chapter 2-4 discussed the electrochemical properties of polymer (PEDOT and PPy) based ternary nanocomposites for supercapacitor applications. It was also discussed that electrode surface can be tuned by swift heavy ion irradiation technique. In the present chapter, the Al^{3+} ion electrochemistry of exfoliated Ti_3AlC_2 MAX phase in aqueous electrolyte is discussed. The advantages of Al^{3+} ion based energy storage systems were explained in the introduction of this thesis.

The discovery of MXenes from MAX phases by the pioneering research group of Gogotsi and Barsoum in the year 2011 has redefined the family of 2D materials and, subsequently, set a resurgent wave of enthusiasm in the research of these materials [1]. MXenes are considered as a novel class of advanced and revolutionary material with extraordinary physicochemical properties [2, 3]. The first and most investigated MXene is $Ti_3C_2T_x$ (T_x represents functional groups). However, more than 30 different types of MXenes have been successfully processed with possible existence of hundreds of MXene phases theoretically [4]. MXenes have received greatest attention in the area of electrochemical energy storage [5-7]. However, studies on the electrochemistry of MXenes for Al^{3+}-ions storage are very limited.

The processing of MXenes involves steps which raise safety concerns. A vast majority of MXenes are processed using HF acid because it can selectively etch the A elements (mostly group 13 and 14 elements of the periodic table) present in the MAX phase [2, 5-9]. It is well-know that HF acid is extremely reactive and it can cause serious and, at times, fatal injuries when comes in contact with human skin. Therefore, stringent and specialized procedures are always followed while handling HF acid to maintain safety. Therefore, there are unrelenting efforts to find alternative approaches avoiding HF acid while processing of MXenes. Electrochemical etching technique may be a novel choice in this context. This particular work discusses a systematic investigation to electrochemically exfoliate MAX phase (Ti_3AlC_2) in a hybrid aqueous electrolyte of $AlCl_3$ and NaOH. We also show that the electrochemically exfoliated MAX phase shows unusual diffusion-controlled Al^{3+} ion

storage behavior in aqueous electrolyte. The phenomenon of Al^{3+} ion storage in exfoliated MAX phase is extremely rare and, hence, this study is important for future expedition of Al^{3+} ion-based energy storage devices.

5.2 Experimental

5.2.1 Materials: Ti_3AlC_2 MAX phase was procured from Nanoshel and was used without any further treatment. Aluminum chloride ($AlCl_3$, Merck), sodium hydroxide (NaOH, Merck) and sodium chloride (NaCl, Merck) were used in different steps of the treatment process. NMP (alfa aesar) and PVDF (sigma-aldrich) were used for electrode preparation.

5.2.2 Electrode preparation: The slurry for electrode preparation was prepared by mixing Ti_3AlC_2 powder (active material) and PVDF in a mass ratio of 70:30 using NMP as medium. Then the slurry was drop coated on Ti foil (1 cm x 1 cm) and dried in oven at 100 ^oC overnight. The mass of active material (Ti_3AlC_2) loaded in the prepared electrodes was approximately 5 mg.

5.2.3 Electrochemical exfoliation process: Electrochemical exfoliation experiments were performed in a conventional symmetric electrochemical cell arrangement (Ti_3AlC_2//Ti_3AlC_2). The schematic of the set-up is shown in Scheme 1. A dc power source was connected to two Ti_3AlC_2 electrodes that were coated on Ti foil. Various dc potentials in the range of 3-8 V were applied. We used different electrolytes for the electrochemical exfoliation process such as aqueous electrolytes of $AlCl_3$, NaOH and mixture of $AlCl_3$ and NaOH. Different concentrations were used and it is noted clearly in the result section below. All the experiments were performed at room temperature and ambient atmosphere.

5.2.4 Structural and morphological characterization: Powder X-ray diffraction technique was used to identify the crystalline phase. Morphology of the investigated materials was examined by Field Emission Scanning Electron Microscopy (FESEM Model: Zeiss sigma 300). Raman spectroscopy was performed with Renishaw basis series with 514 nm laser excitation wavelength and LASER power of 10mW.

5.2.5 Electrochemical measurements: Cyclic voltammetry (CV) and galvanostatic charge/discharge (GCD) measurements were investigated in conventional three electrodes arrangement. The three electrodes were: 1 M KCl electrolyte containing Ag/AgCl (reference electrode), platinum wire (counter electrode) and active material deposited Ti foil (working electrode). CV and GCD were carried out in 1 M H_2SO_4 and 1 M $AlCl_3$ electrolytes. The EIS data were recorded in Biologic SP-300 in the frequency range of $3x10^6$ Hz to 1 Hz at a bias potential of 10 mV.

5.3 Results and discussion

The crystallographic identification of Ti_3AlC_2 was performed by XRD measurement and the XRD pattern is shown in Figure 5.1a. The XRD pattern reflects peaks at 2θ = 9.6º, 19.2º, 34º, 36.16º, 39.08º, 41.8º, 44.89º, 48.63º, 52.38º, 56.5º, 60.6º (JCPDS no. 52-0875), which are characteristic peaks of Ti_3AlC_2. The morphology of Ti_3AlC_2 was examined by FESEM and the very compact yet stacked layered structure of Ti_3AlC_2 could be noticed from the FESEM micrographs (Figure 5.1b). This is similar to the MAX phase reported by various research groups [10-12].

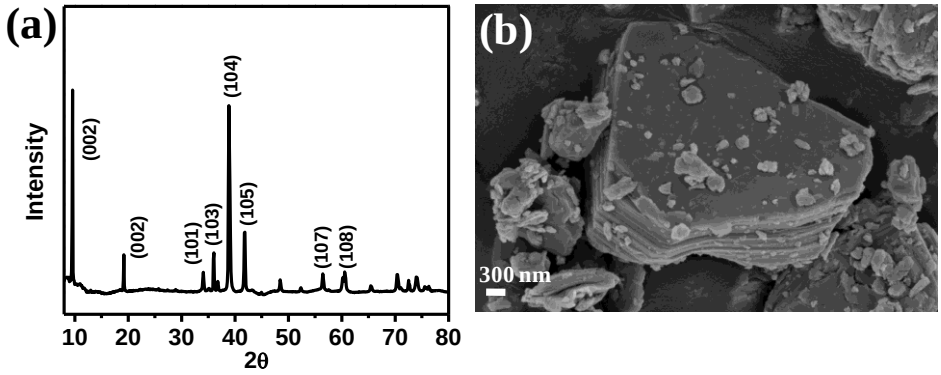

Figure 5.1: (a) XRD pattern and (b) FESEM image of pristine Ti_3AlC_2

To verify any possible electrochemical activity of the selected MAX phase, cyclic voltammetry (CV) and galvanostatic charge/discharge experiments were performed in 1 M H_2SO_4 and 1 M $AlCl_3$ aqueous electrolytes. These are shown in figure 5.2 (a, b). It is noticed from the CV profiles that the pristine MAX phase shows no definite electrochemical activity in both the electrolytes which is again corroborated by the charge/discharge experiments, where no noticeable specific capacitances could be estimated (figure 5.2 c, d). With this basic but important information in hand, we embarked on to perform our exfoliation experiments.

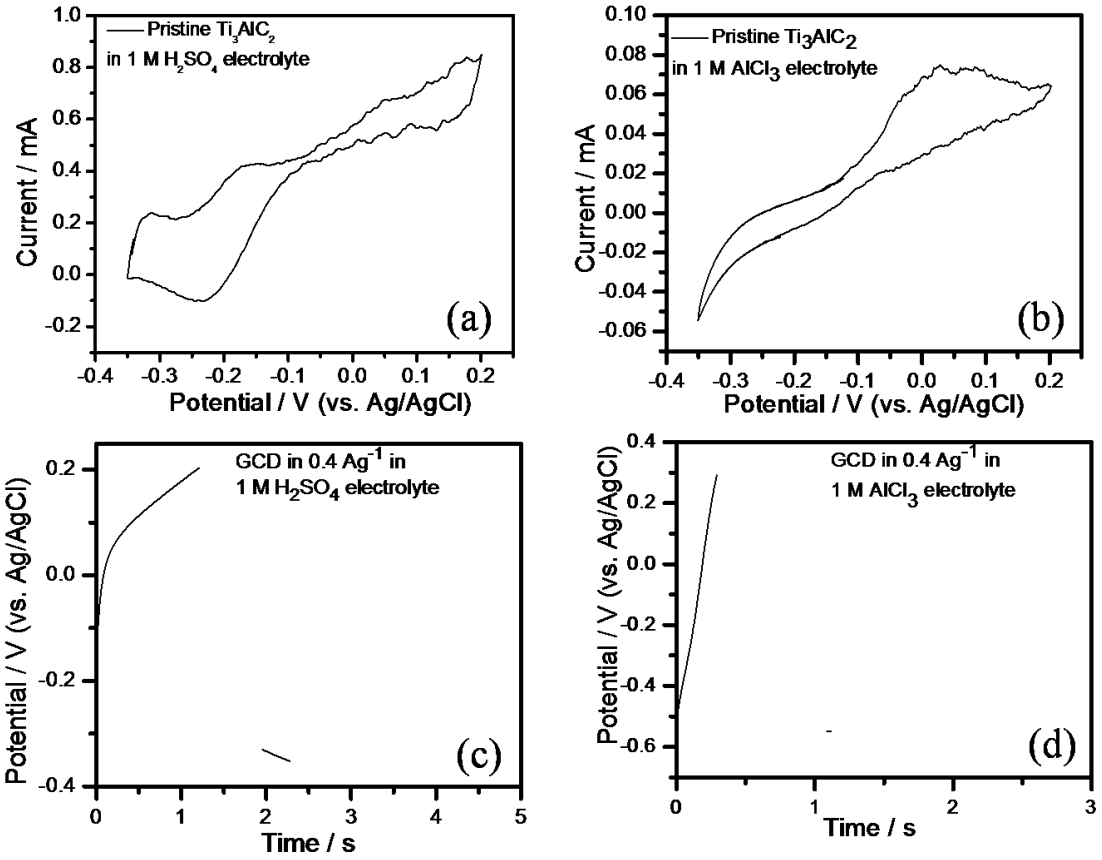

Figure 5.2: Cyclic voltammetry of Ti_3AlC_2 in (a) 1 M H_2SO_4 and (b) 1 M $AlCl_3$ aqueous electrolyte; Galvanostatic charge/discharge measurements of Ti_3AlC_2 in (c) 1 M H_2SO_4 and (d) 1 M $AlCl_3$ aqueous electrolyte.

Our first choice of electrolyte for the exfoliation process is an aqueous electrolyte of $AlCl_3$ (1 M). Recently, our group demonstrated exfoliation of graphite to achieve graphite nanoflakes by a similar electrochemical method in aqueous $AlCl_3$ electrolyte by applying a dc potential of 3-5 V [13]. Inspired by it, we followed a similar protocol to electrochemically treat the MAX phase. Initially, the electrochemical treatment was performed in 1 M $AlCl_3$ electrolyte for a duration of 10 minute for different applied dc potentials (3-8 V). After performing the electrochemical treatment, CV experiments were pursued with both the treated electrodes (connected to the positive and negative terminals) in 1 M H_2SO_4 and 1 M $AlCl_3$ aqueous electrolytes. Figure 5.3 (a-c) shows the respective CV profiles in H_2SO_4. As could be observed, there is no significant change in the CV profiles of the electrode connected to the negative terminal of the power supply in comparison

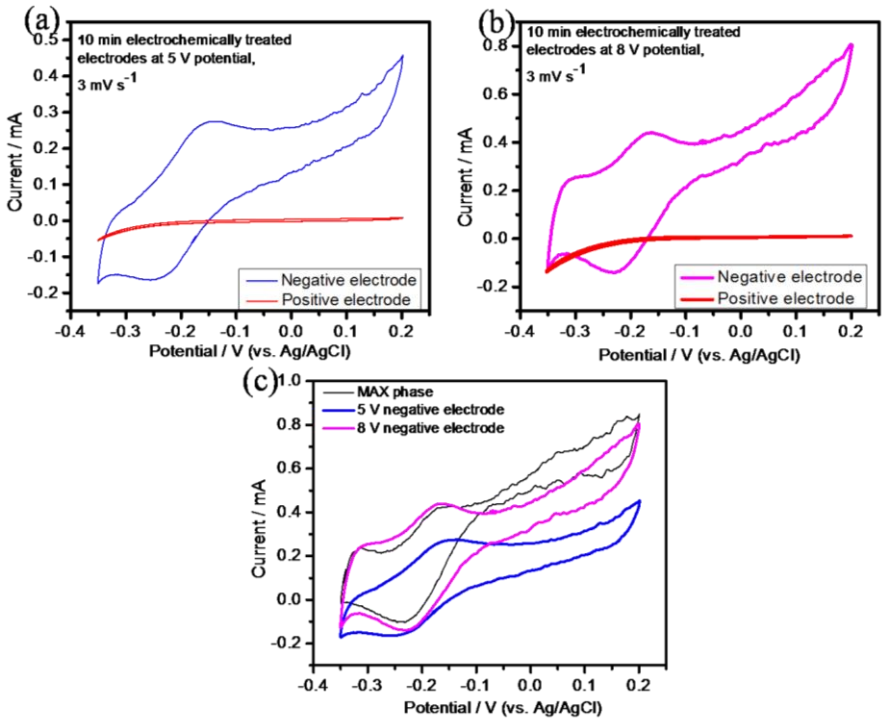

Figure 5.3: CV measurements in 1 M H_2SO_4 electrolyte for Ti_3AlC_2 electrodes treated in 1 M $AlCl_3$ for 10 min for both positive and negative electrodes. Treatment potentials are (a) 5 V and (b) 8 V; (c) comparison of CV profiles of negative electrode with pristine Ti_3AlC_2 for 3 mVs^{-1} scan rate.

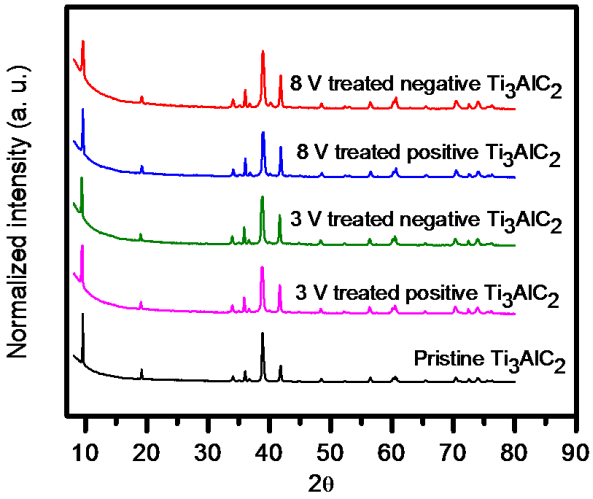

Figure 5.4: XRD patterns of pristine Ti_3AlC_2, and both positive and negative Ti_3AlC_2 electrodes treated in 1 M $AlCl_3$ electrolyte at 3 V and 8 V potentials.

to the pristine MAX phase, but the area under the CV curve of the positive electrode observed to be decreased significantly. The XRD patterns for the treated electrodes

also showed no noticeable changes in the crystal structure in comparison to the pristine MAX phase (Figure 5.4).

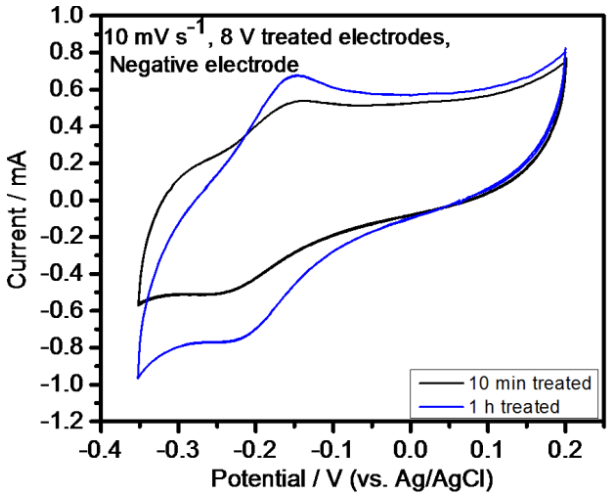

Figure 5.5: CV measurements in 1 M H_2SO_4 electrolyte for Ti_3AlC_2 negative electrodes treated in 1 M $AlCl_3$ electrolyte at 8 V for a duration of 10 min and 1 h.

A marginal improvement in CV current could be seen by increasing the electrochemical treatment time from 10 min to 1 h (Figure 5.5). Similar trends in electrochemical activity could also be observed for $AlCl_3$ aqueous electrolyte (Figure 5.6). Overall, it could be inferred that there is no influence of the electrochemical treatment on the MAX phase in $AlCl_3$ electrolyte.

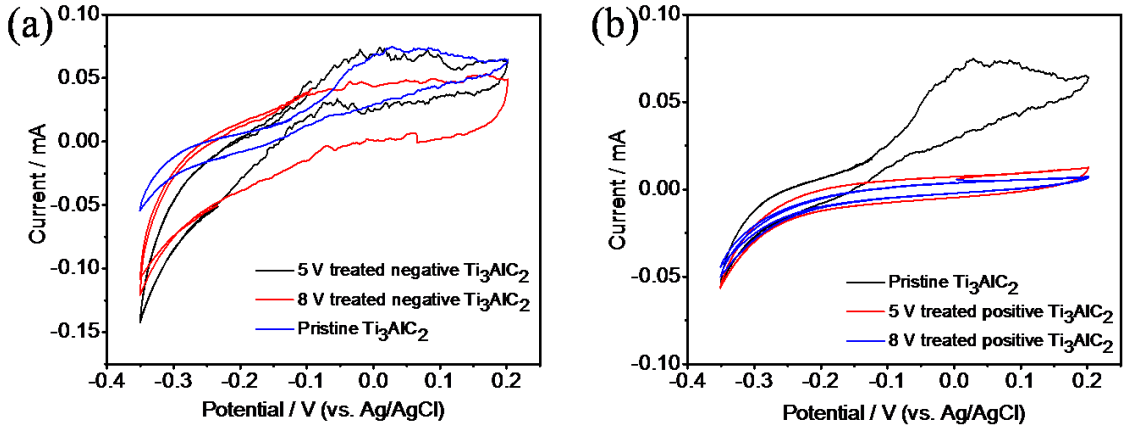

Figure 5.6: CV in 1 M $AlCl_3$ electrolyte. (a) Pristine and negative electrode, (b) pristine Ti_3AlC_2 positive electrode treated in 5 V and 8 V dc potential.

Our second strategy is inspired by the preparation of nanotubes utilizing porous anodic alumina membrane. The nanotube could be prepared by dissolution of

the alumina membrane and for this purpose, the most commonly used medium is concentrated NaOH solution [14, 15]. Therefore, we employed 5 M (pH = 14.7), 10 M (pH = 15) and 12.5 M (pH = 15.1) NaOH solutions for the electrochemical exfoliation of Ti_3AlC_2 MAX phase. Initially, we electrochemically treated the Ti_3AlC_2 electrodes in 5 M NaOH for 2 h at an applied dc potential of 8 V. With the treated electrodes, CV experiments were again performed in 1 M H_2SO_4 electrolyte.

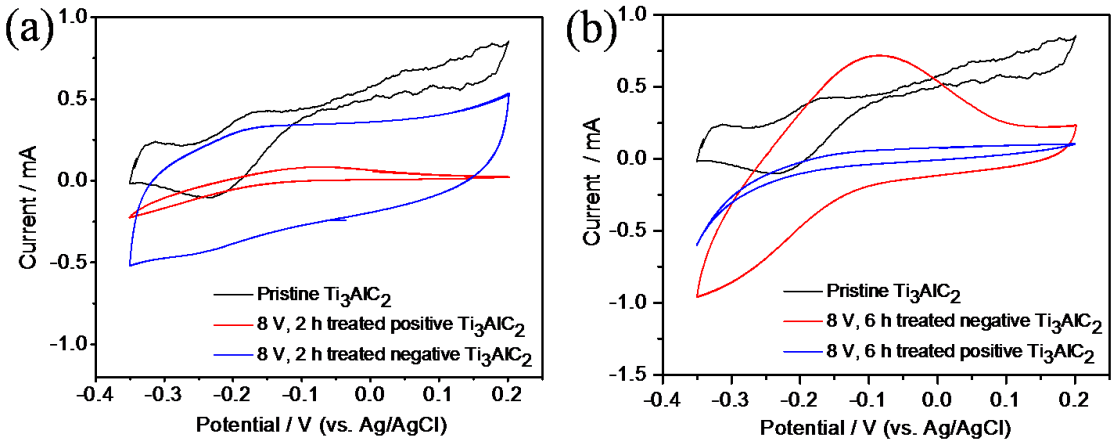

Figure 5.7: CV measurements taken in 1M H_2SO_4 for Ti_3AlC_2 electrodes treated in 5 M NaOH electrolyte for (a) 2 h and (b) 6 h at 8 V power supply.

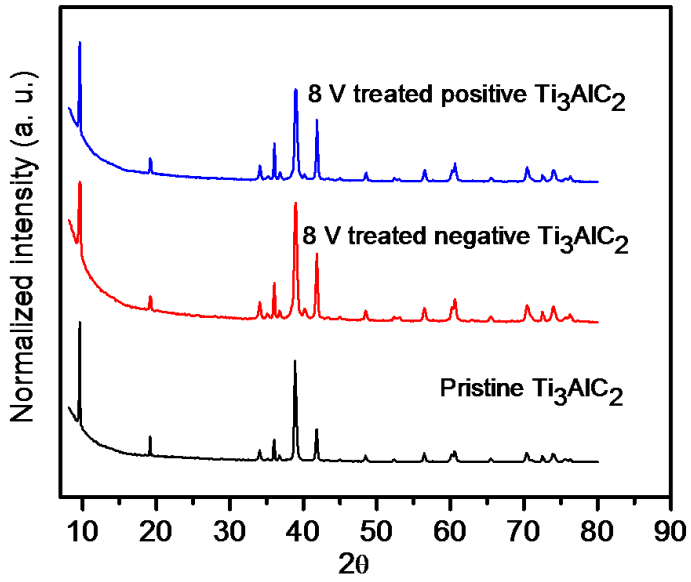

Figure 5.8: XRD of Ti_3AlC_2 treated in 5 M NaOH electrolyte for 6 h.

As could be seen from the figure 5.7a, a slight improvement is observed in electrochemical active area. The estimated capacitance value is 8.7 Fg^{-1} in comparison to 4.05 Fg^{-1} for pristine MAX phase. An improvement in CV profile has been observed when the treatment time has increased to 6 h (Figure 5.7 b). In this case also

the positive terminal electrode shows diminished electrochemical behavior. The XRD patterns of the NaOH treated electrodes also did not show any difference in comparison to pristine MAX phase (Figure 5.8). We also increased the electrochemical treatment time from 6 h to 12 h to see any change in electrochemical activity. It is realized that there is a decrease in electrochemical activity for 12 h treated electrode than that of 6 h treated electrode (Figure 5.9). Henceforth, we decided to electrochemically treat all samples at 8 V for a duration of 6 h until and unless categorically mentioned.

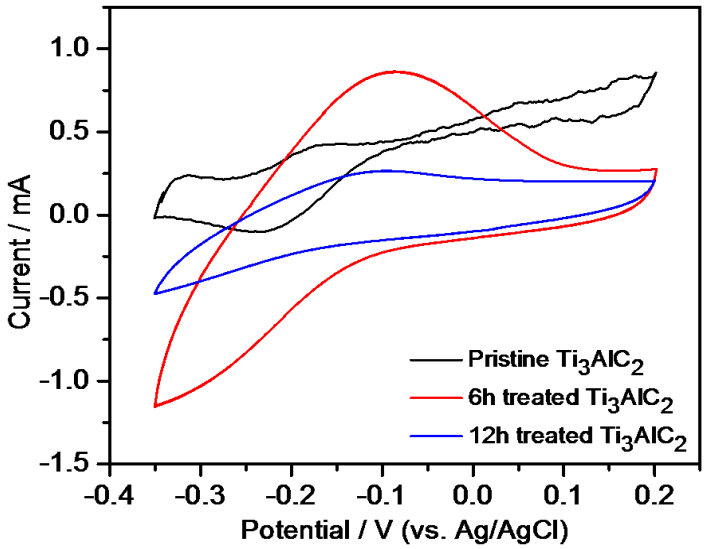

Figure 5.9: CV profiles in 1 M H_2SO_4 for the following electrodes: pristine Ti_3AlC_2, 6 h treated (in 5 M NaOH electrolyte) Ti_3AlC_2 and 12 h treated (in 5 M NaOH electrolyte).

Next, we changed the concentration of the electrolyte from 5 M NaOH to 10 M NaOH while performing the electrochemical treatment of the Ti_3AlC_2 electrodes. The electrodes treated with 10 M NaOH electrolyte possess improved electrochemical activity than that of 5 M NaOH treated electrode (Figure 5.10 a). The capacitance value is estimated to be 18 Fg^{-1}. In this case also however, the XRD patterns of the treated electrodes are similar to the pristine MAX phase (Figure 5.10 b). We further increased the concentration of NaOH to 12.5 M. It is noted here that a clear solution could not be prepared beyond 12.5 M at room temperature. Therefore, we restricted our experiments with 12.5 M NaOH. The electrode treated in 12.5 M NaOH electrolyte showed electrochemical activity similar to 10 M NaOH treated electrode in 1 M H_2SO_4 electrolyte (Figure 5.11).

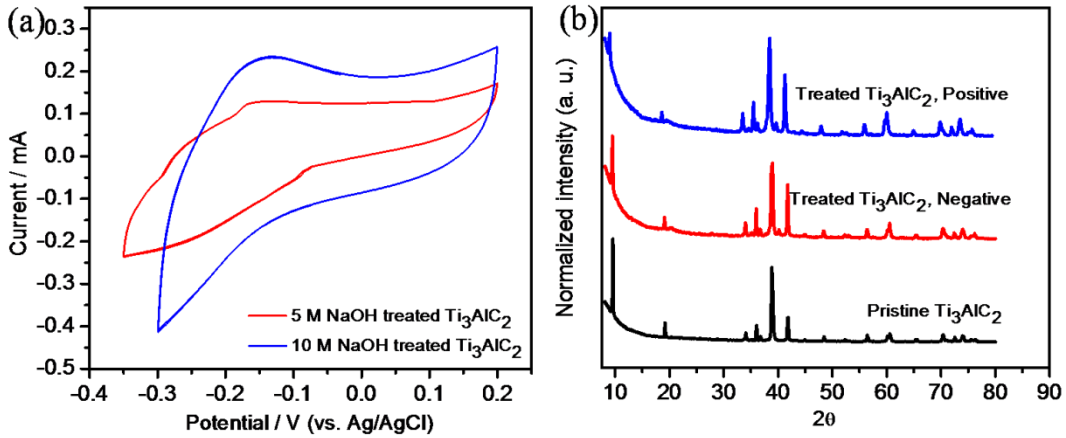

Figure 5.10: (a) CV profiles in 1 M H_2SO_4 for the following electrodes: 5 M and 10 M NaOH electrolyte treated Ti_3AlC_2 electrodes, Duration = 6 h and (b) XRD patterns of Ti_3AlC_2 treated in 8V potential for 6h at 10M NaOH electrolyte.

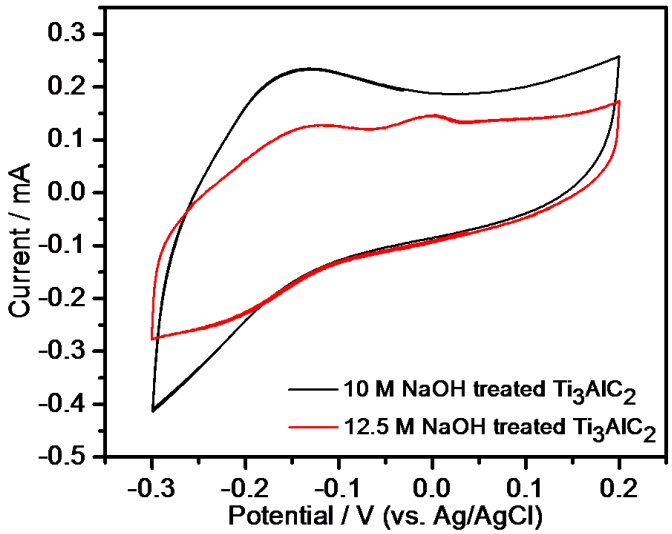

Figure 5.11: CV profiles in 1 M H_2SO_4 for the following electrodes: 10 M and 12.5 M NaOH electrolyte treated Ti_3AlC_2 electrodes, Duration = 6 h.

Our third strategy was to use a hybrid electrolyte of $AlCl_3$ and NaOH to electrochemically treat the MAX phase. The electrolyte that was first used was basically a mixture of 1 M $AlCl_3$ and 5 M NaOH aqueous solutions (1:10 v/v). The applied dc potential was 8 V for 6 h. After the electrochemical treatment, CV experiment was performed with this treated Ti_3AlC_2 electrode in 1 M H_2SO_4 electrolyte and the CV profile is shown in figure 5.12 a. This electrode also didn't show any electrochemical activity. Further, CV experiment was performed with 1 M

$AlCl_3$ aqueous electrolyte. To our utter surprise, a pair of prominent redox peaks could be noticed in the CV profiles. The cathodic (peak A) and anodic (peak B) peaks are located respectively at potentials of -1.11 V and -1.08 V (Figure 5.2 b). In addition, there are also two very small intensity redox peaks (peak C and D) at -1.02 V and -1.04 V (Figure 5.12 b). An irreversible broad cathodic peak at -0.85 V was also observed. The scan rate was 1 mVs^{-1}. For clarity, it is appropriate to note here again that the pristine MAX phase does not show any electrochemical activity in 1 M $AlCl_3$ electrolyte (figure 5.2 b).

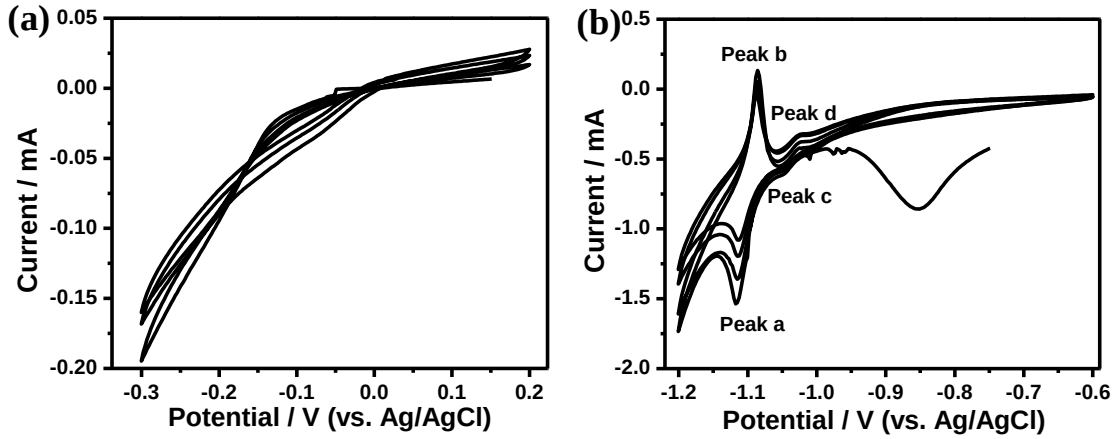

Figure 5.12: Cyclic voltammetry of Ti_3AlC_2 electrodes treated in hybrid electrolyte (1 M $AlCl_3$ / 5 M NaOH) in (a) 1 M H_2SO_4 and (b) 1 M $AlCl_3$ aqueous electrolyte at the scan rate of 1 mVs^{-1}.

Galvanostatic charge/ discharge (GCD) experiment was also performed with this electrochemically treated Ti_3AlC_2 electrode in 1 M $AlCl_3$ electrolyte. While the pristine Ti_3AlC_2 MAX phase could not be galvanostatically cycled at all any current rates (figure 5.2 c, d), the electrochemically treated electrode could now be cycled (Figure 5.13 a). The current densities are 0.4 Ag^{-1} and 0.02 Ag^{-1} for the discharge and charge cycles respectively. The variation of capacitance with cycle number is shown in figure 5.13 b and it is seen that discharge capacitance values of 17 Fg^{-1} was obtained. The stability of the treated electrode was evaluated for 1000 cycles and it was found that electrode possesses 82% of discharge stability after 1000 cycles (Figure 5.13 c, d). The current rates in this case were 1 Ag^{-1} for discharging and 0.02 Ag^{-1} for charging.

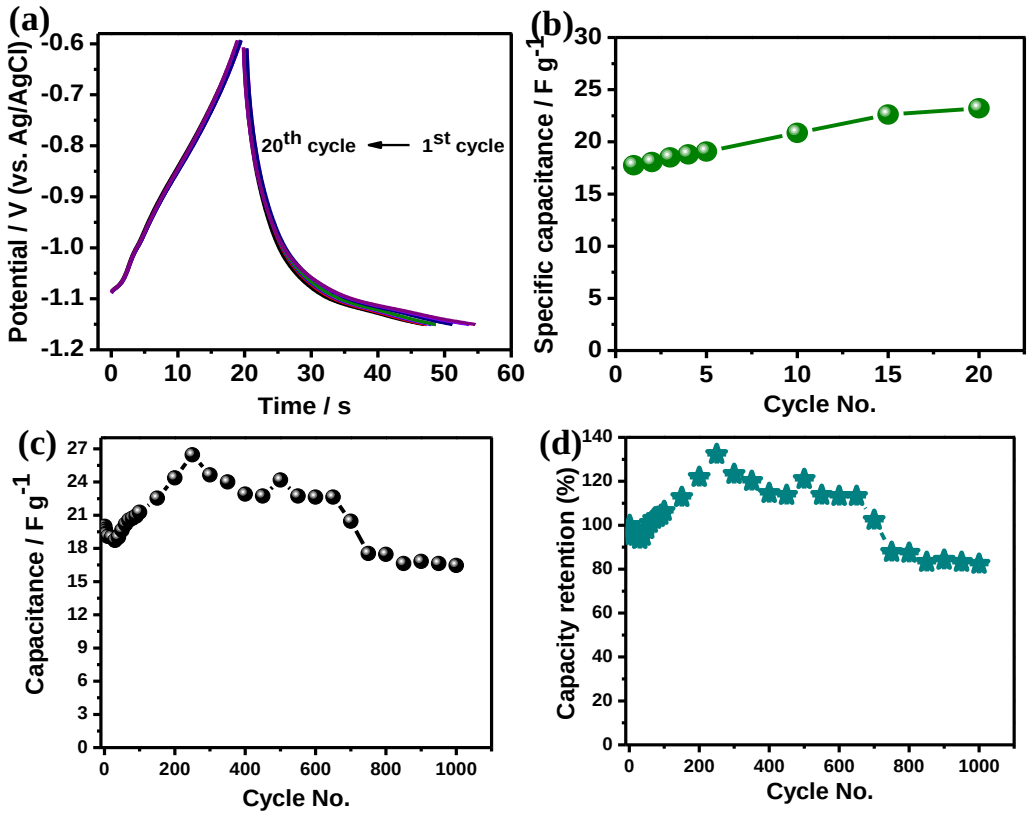

Figure 5.13: Electrochemical measurements of Ti_3AlC_2 electrodes treated in hybrid electrolyte (1 M $AlCl_3$ / 5 M NaOH) (a) galvanostatic charge/discharge measurements in 1 M $AlCl_3$ aqueous electrolyte, (b) specific capacitance vs. cycle numbers at current densities of 0.4 Ag^{-1} and 0.02 Ag^{-1} for discharge and charge cycles respectively, (c) capacitance versus cycle numbers and (d) capacity retention (%) vs. cycle numbers for 1000 repeated GCD cycles in 1 M $AlCl_3$ aqueous electrolyte at 1 Ag^{-1} and 0.02 Ag^{-1} for discharge and charge cycles respectively .

Thereafter, we changed the NaOH concentration while treating the MAX phase. Now, the electrolyte is a mixture of 1 M $AlCl_3$ and 12.5 M NaOH aqueous solutions (1:10 v/v). In this case also, the CV profiles show redox peaks at potentials of -1.08 V and -1.11 V are prominently visible (Figure 5.14 a, b). An enhanced specific capacitance value of 49.3 Fg^{-1} for the 1st cycle (current rate is 0.4 Ag^{-1}) could be estimated in this case from charge-discharge profiles (Figure 5.14 c). However, due to unknown reasons to us, the experiment could not be performed for a large number of cycles (Figure 5.14 d). It appears that some side reactions take place because of which the discharge curve could not be completed.

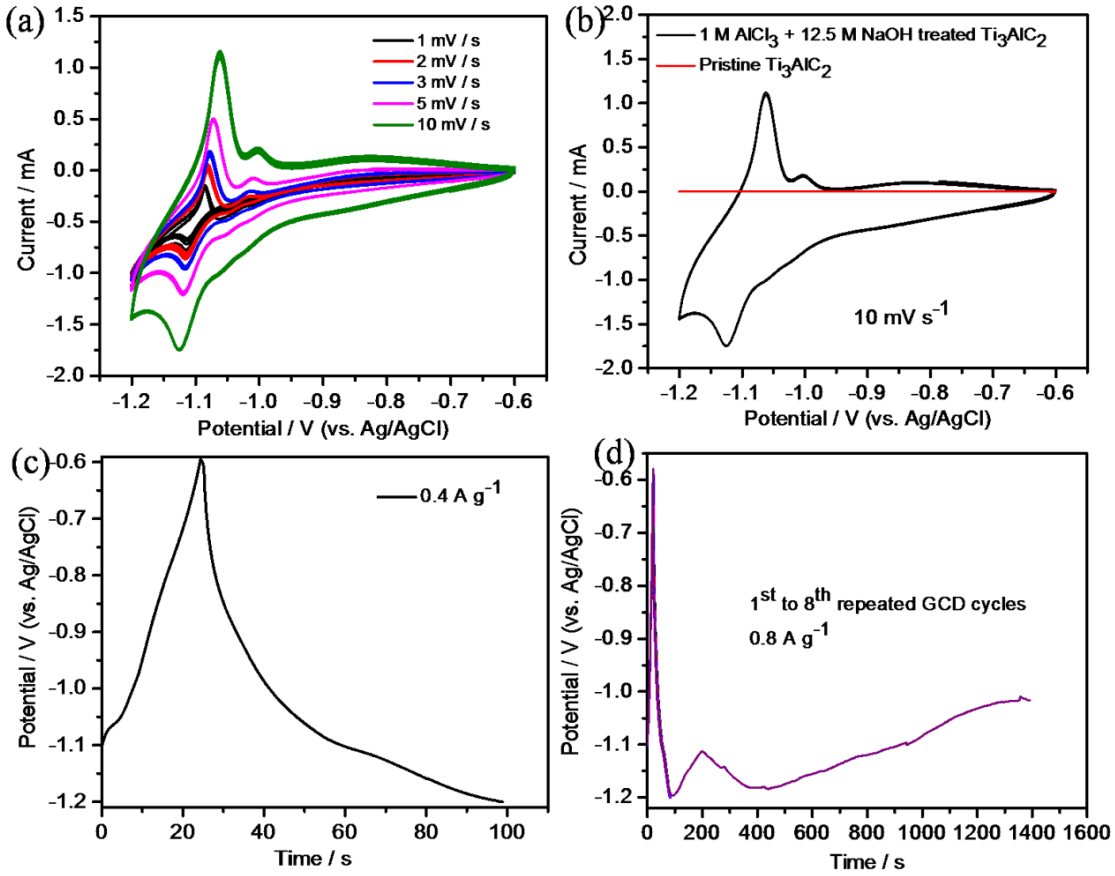

Figure 5.14: (a) CV profiles of Ti_3AlC_2 electrodes treated in1 M $AlCl_3$ added 12.5 M NaOH hybrid electrolyte. The CV was performed in 1 M $AlCl_3$ aqueous electrolyte at scan rates of 1 $mVs^{-1}$to 10 mVs^{-1}, (b) Comparison of CV profiles of pristine $Ti_3AlC_2$and Ti_3AlC_2 electrodes treated in1 M $AlCl_3$ added 12.5 M NaOH hybrid electrolyte. The CV was performed in 1 M $AlCl_3$ electrolyte, and (c, d) GCD measurements in 1 M $AlCl_3$ electrolyte for Ti_3AlC_2 electrodes treated with 1 M $AlCl_3$ added 12.5 M NaOH electrolyte.

In addition, the pristine MAX phase electrode was also treated with NaCl instead of $AlCl_3$. That means the electrolyte used for electrochemical treatment is now a mixture of 1 M NaCl and 5 M NaOH aqueous electrolytes. The comparison of the CV profiles of these two electrodes (i.e. one treated with 1 M NaCl/ 5 M NaOH and another 1 M $AlCl_3$/ 5 M NaOH electrolytes) clearly indicates that the electrochemical effects are prominent only in the case of $AlCl_3$ treated electrolytes (Figure 5.15).

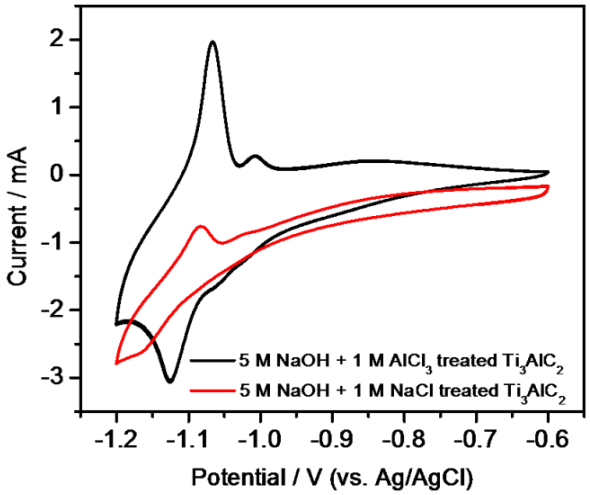

Figure 5.15: CV measurements in 1 M $AlCl_3$ electrolyte for Ti_3AlC_2 electrodes treated in 1 M $AlCl_3$ added 5 M NaOH and 1 M NaCl added 5 M NaOH electrolytes.

To better understand the Al^{3+} ion kinetics of the treated Ti_3AlC_2 electrode (with 1 M $AlCl_3$ added 5 M NaOH), CV experiments were performed at different scan rates ranging from 1 to 10 mVs^{-1} and it is shown in Figure 5.16 a. Generally, for diffusion-controlled process, the current response is proportional to the square root of the scan rates as per Randles-Sevcik equation [16]. Therefore, variations of cathodic and anodic peak currents were plotted with the square root of scan rates and shown in Figure 5.16 b. We found that all of the redox peaks, as indicated in the figure 5.16 a, follow a linear relationship with the square root of the scan rates signifying a diffusion dominated process. The quantitative estimation of the diffusion process is further performed using the following equation (5.1, 5.2):

$$i(V) = K_1\vartheta + K_2\vartheta^{\frac{1}{2}} \tag{5.1}$$

$$\frac{i(V)}{\vartheta^{\frac{1}{2}}} = K_1\vartheta^{\frac{1}{2}} + K_2 \tag{5.2}$$

Here, the term $K_1\vartheta$ gives the capacitive part and $K_2\vartheta^{\frac{1}{2}}$ gives the diffusive contribution to the overall storage process. It is again found that diffusion process is dominant and the diffusive contribution is as high as 73% (measured at the scan rate of 1 mVs^{-1}) (Figure 5.16 c, d). Therefore, it could be commented that the electrochemical activity is mainly attributed to the Al^{3+} ion intercalation and deintercalation process.

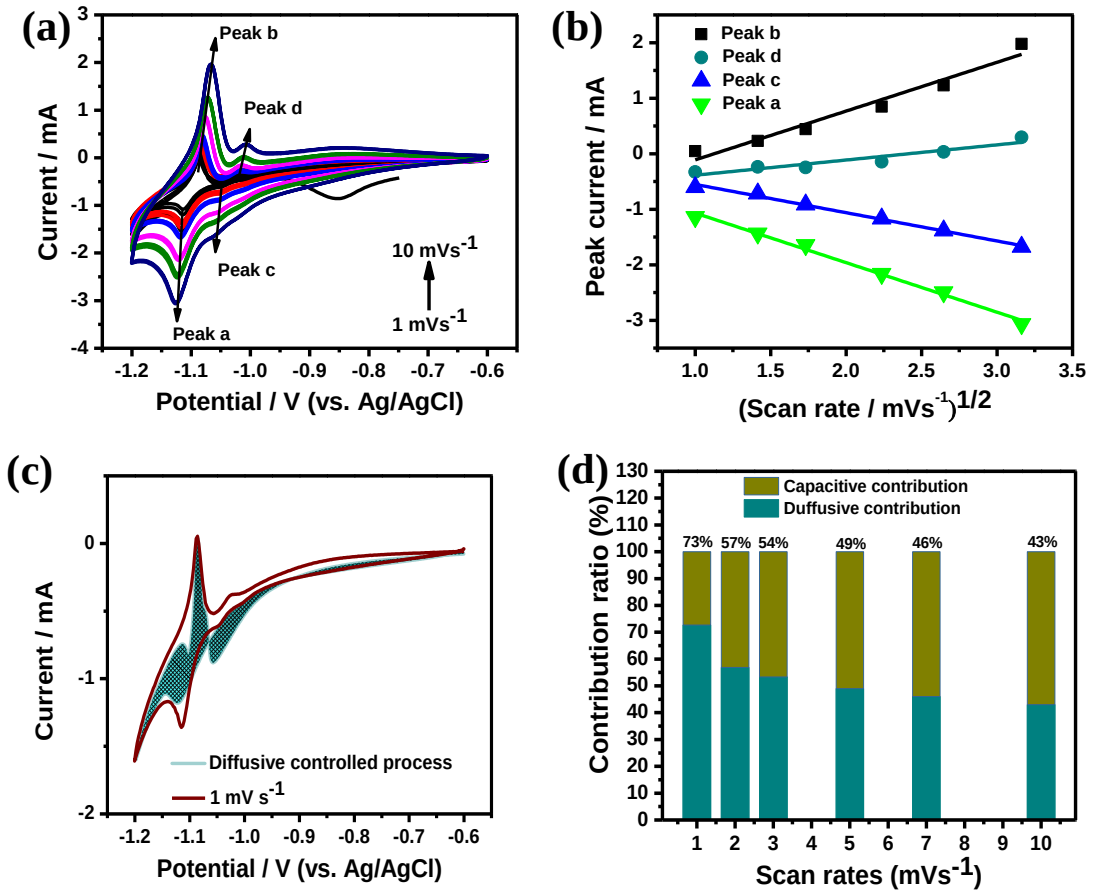

Figure 5.16: Electrochemical measurements of Ti_3AlC_2 electrodes treated in hybrid electrolyte (1 M $AlCl_3$ / 5 M NaOH) (a) Cyclic voltammetry in 1 M $AlCl_3$ aqueous electrolyte at scan rates of 1 to 10 mVs^{-1}, (b) variation of peak currents with square root of scan rates, (c) area separation under CV curve for diffusive controlled processes at 1 mVs^{-1} of scan rate and (d) relative contribution of diffusive and capacitive controlled charge storage processes at different scan rates.

To verify any changes in the morphology of the MAX phase after electrochemical treatment, we examined few of the treated electrodes by FESEM (Figure 5.17). As already mentioned the pristine Ti_3AlCl_2 possesses a compact yet stacked layered structure (Figure 5.17 a). The surface of 5 M NaOH treated electrode shows presence of foam like structure, but exfoliation could not be observed (Figure 5.17 d). Similarly, exfoliation could not be seen in case of electrodes treated with 1 M $AlCl_3$ added 1 M NaOH (Figure 5.17 e, f). Most strikingly, exfoliation could be noticed for the electrodes treated with 1 M $AlCl_3$ added 5 M NaOH electrolyte (Figure

5.17 b, c). In addition, the surface of the exfoliated layers is also found to be porous. And this latter electrode shows the Al^{3+} ion storage behavior.

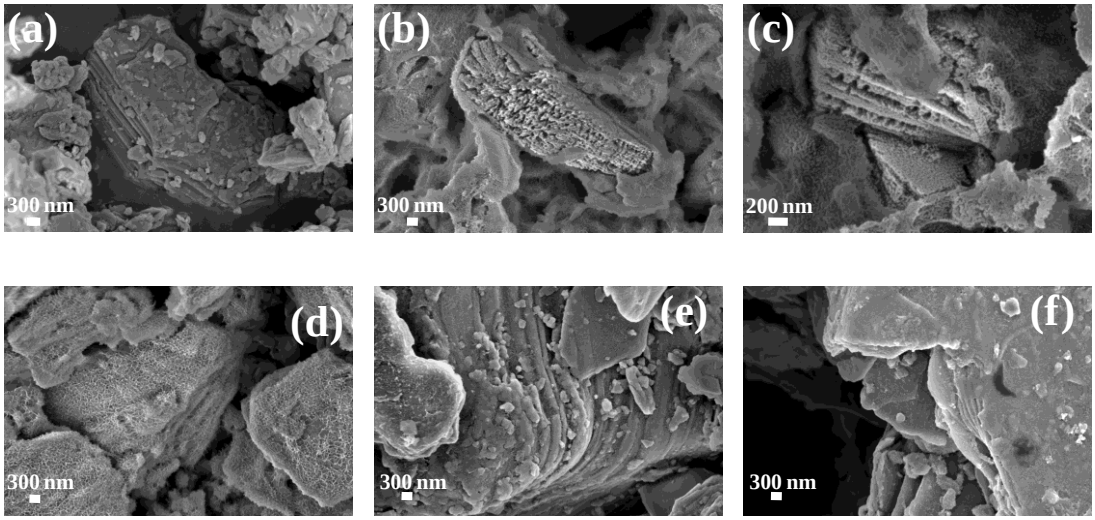

Figure 5.17: FESEM images of (a) pristine Ti_3AlC_2, (b, c) Ti_3AlC_2 electrodes treated in hybrid electrolyte (1 M $AlCl_3$ / 5 M NaOH), (d) 5 M NaOH treated Ti_3AlC_2 electrode, and (e, f) Ti_3AlC_2 electrode treated in hybrid electrolyte (1 M $AlCl_3$ / 1 M NaOH).

The XRD pattern of this treated electrode (1 M $AlCl_3$ added 5 M NaOH) also shows a difference in comparison to the pristine Ti_3AlCl_2. In this case, the diffraction peak at $2\theta = 9.6^o$ vanished completely (Figure 5.18 a). The similar trend is also observed for electrochemically treated electrode with 1 M $AlCl_3$ added 12.5 M NaOH electrolyte (Figure 5.18 a). However, when the NaOH concentration was lowered (i.e. 1 M), the peak could be noticed though small in intensity. The electrochemically treated electrodes were also examined using Raman spectroscopy with 514 nm excitation wavelength. The Raman spectra are shown in Figure 5.18 b. The pristine Ti_3AlC_2 possesses the characteristic Raman signals marked as peak I-VI in the range of 100 to 800 cm^{-1} [1, 17]. The peak of MAX phase at 270 cm^{-1} is referred to A_{1g} (Ti, Al) vibration and the peak at 660 cm^{-1} corresponds to out-of-plane vibration (Ti, C) [18]. In contrast, the Raman spectrum of electrochemically treated electrode with 1 M $AlCl_3$ added 5 M NaOH electrolyte is quite different from the pristine MAX phase and bears complex features. It is seen that the peak intensity of the first three peaks (I, II and III) diminished completely. Similar trend was also observed by the group of Gogotsi [1]. In addition, the peak at 660 cm^{-1} (peak VI) is showing red shift after

electrochemical treatment and the new peak is appearing at 725 cm^{-1}. Gogotsi et al. concluded that this kind of change in the Raman spectra may be a result of selective etching of MAX phase [17].

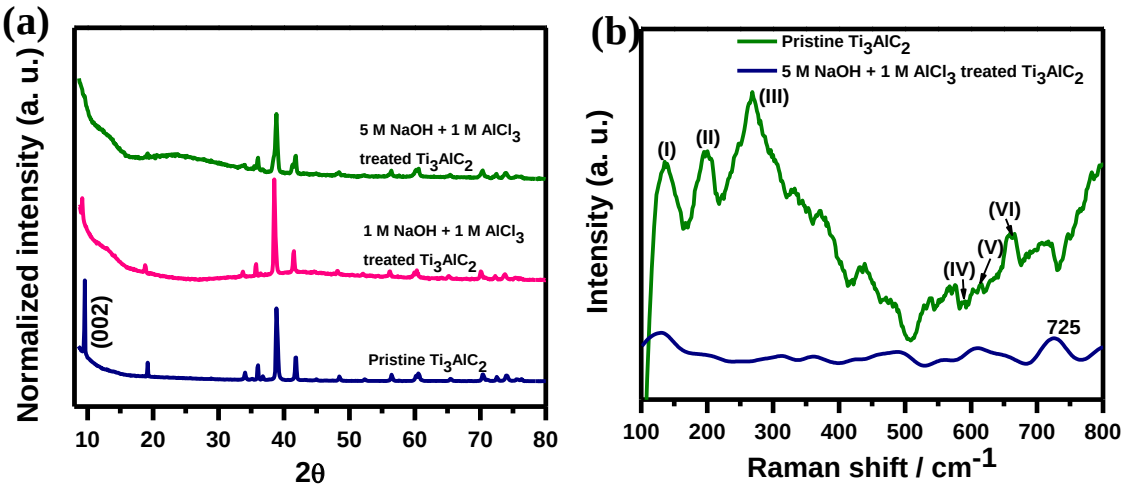

Figure 5.18: (a) XRD patterns and (b) Raman spectra of pristine Ti_3AlC_2 and Ti_3AlC_2 treated in hybrid electrolyte ($AlCl_3$ / NaOH).

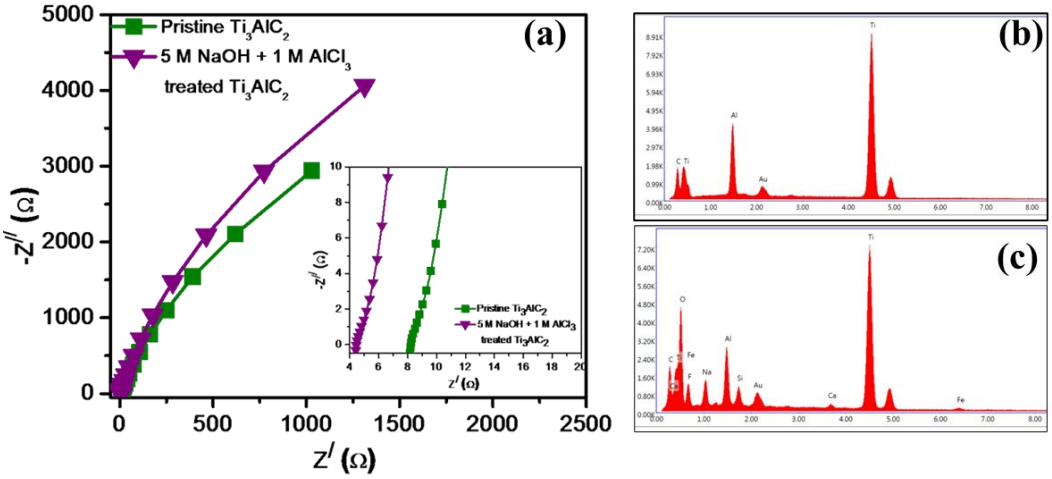

Figure 5.19: (a) Nyquist plots of pristine Ti_3AlC_2 and hybrid electrolyte (in 5 M NaOH + 1 M $AlCl_3$) treated Ti_3AlC_2 electrodes, inset shows the zoomed portion in the high frequency region; EDX spectra of (b) Ti_3AlC_2, and (c) hybrid electrolyte (in 5 M NaOH + 1 M $AlCl_3$) treated Ti_3AlC_2 electrodes.

Additionally, Electrochemical Impedance Spectroscopy (EIS) of pristine Ti_3AlC_2 and treated electrode (1 M $AlCl_3$ added 5 M NaOH electrolyte) was performed in the frequency range of 3 MHz to 1 Hz and the spectra are shown in Figure 5.19. The x-axis intercept of the curve at high frequency region defines

equivalent series resistance (R_s) which is the measure of intrinsic resistance of the electrode and electrolyte's ionic resistance. It was found that R_s value for the electrochemically treated electrode (4.4 Ω cm^{-2}) is lower than the pristine Ti_3AlC_2 electrode (8.1 Ω cm^{-2}). EDX spectra of the pristine Ti_3AlC_2 and treated electrode (1 M $AlCl_3$ added 5 M NaOH electrolyte) is shown in Figure 5.19 (b, c). The atomic % of Al in pristine Ti_3AlC_2 is 14.5 and 5.06 for the treated electrode (1 M $AlCl_3$ added 5 M NaOH electrolyte).

The probable mechanism of formation of exfoliated Ti_3AlC_2 from Ti_3AlC_2 is depicted in Scheme 5.I. Water molecule splits into highly reactive free radicals OH^- and O^- in presence of applied potential. In the 1st step, these free radicals attack the carbon atoms of Ti_3AlC_2. Some of carbon atoms could be removed from Ti_3AlC_2 layered structure by the highly reactive free radicals and open paths for Cl^- ions of the

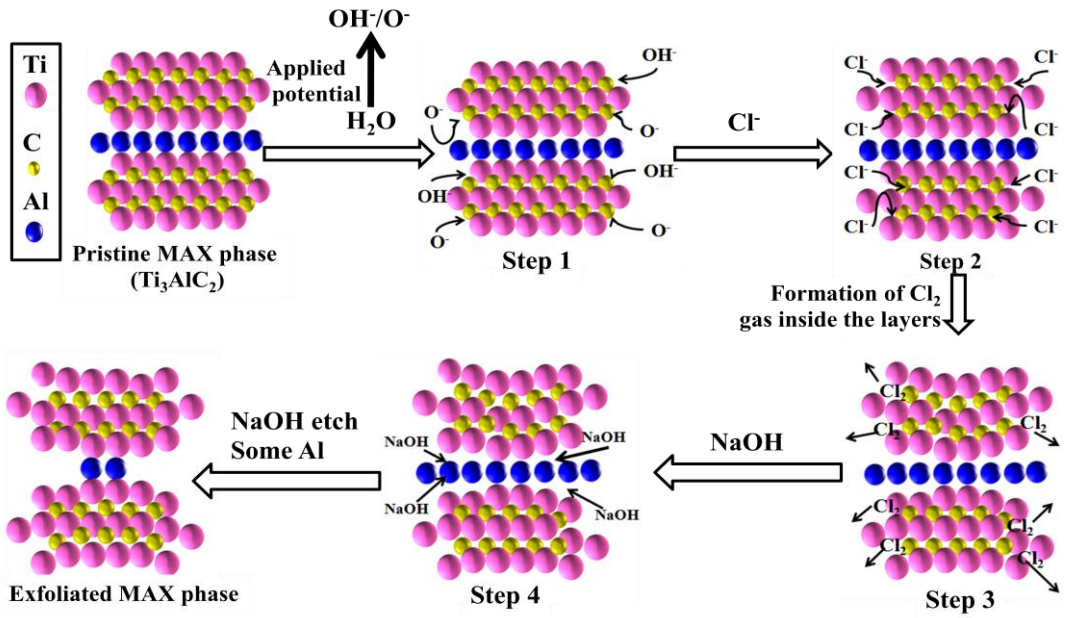

Scheme 5.I: Probable mechanism for exfoliation of MAX phase with the hybrid electrolyte (1 M $AlCl_3$ added 5 M NaOH).

hybrid electrolyte (1 M $AlCl_3$ added 5 M NaOH). Now Cl^- ions can penetrate inside the layered structure [19, 20]. In the next step, Cl^- ions form Cl_2 gas inside the layers and escapes from the material. In this escape process, the layered material gets exfoliated to some extent, leaving paths for NaOH to react with Al atoms of Ti_3AlC_2. At this step, etching occurs at the Al layer.

5.4 Conclusion

In summary, we demonstrated an electrochemical method to exfoliate Ti_3AlC_2 MAX phase in a hybrid aqueous electrolyte of $AlCl_3$ and NaOH. It is interestingly revealed that neither an aqueous solution of $AlCl_3$ nor NaOH alone could help in the exfoliation process. The exfoliation is verified by XRD, FESEM and Raman spectroscopy measurements. While the exfoliated MAX phase does not show any electrochemical activity in commonly used H_2SO_4 electrolyte, it exhibits unusual redox behavior in Al^{3+} ion aqueous electrolyte and the Al^{3+} ion storage process is found to be diffusion limited. Such a behavior was not seen earlier.

5.5 References

[1] Naguib, M., Kurtoglu, M., Presser, V., Lu, J., Niu, J., Heon, M., Hultman, L., Gogotsi, Y., and Barsoum, M.W. Two dimensional nanocrystals produced by exfoliation of Ti_3AlC_2. *Advanced materials*, *23*(37): 4248-4253, 2011.

[2] Ronchi, R.M., Arantes, J.T., and Santos, S.F. Synthesis, structure, properties and applications of MXenes: current status and perspectives. *Ceramics International*, *45*(15): 18167-18188, 2019.

[3] Gogotsi, Y., and Anasori, B. The rise of MXenes. *ACS nano*, *13*(8): 8491-8494, 2019.

[4] Anasori, B. and Gogotsi, Û.G. *2D metal carbides and nitrides (MXenes)*. Springer, Berlin, 416, 2019.

[5] Lukatskaya, M.R., Mashtalir, O., Ren, C.E., Dall'Agnese, Y., Rozier, P., Taberna, P.L., Naguib, M., Simon, P., Barsoum, M.W., and Gogotsi, Y. Cation intercalation and high volumetric capacitance of two-dimensional titanium carbide. *Science*, 341(6153): 1502-1505, 2013.

[6] Ghidiu, M., Lukatskaya, M.R., Zhao, M.Q., Gogotsi, Y., and Barsoum, M.W. Conductive two-dimensional titanium carbide 'clay' with high volumetric capacitance. *Nature*, 516(7529): 78-81, 2014.

[7] Li, X., Huang, Z., Shuck, C.E., Liang, G., Gogotsi, Y., and Zhi, C. MXene chemistry, electrochemistry and energy storage applications. *Nature Reviews Chemistry*, 1-16, 2022.

[8] Naguib, M., Mashtalir, O., Carle, J., Presser, V., Lu, J., Hultman, L., Gogotsi, Y., and Barsoum, M.W. Two-dimensional transition metal carbides. *ACS nano*, *6*(2):1322-1331, 2012.

[9] Nguyen, V.H., Nguyen, B.S., Hu, C., Nguyen, C.C., Nguyen, D.L.T., Nguyen Dinh, M.T., Vo, D.V.N., Trinh, Q.T., Shokouhimehr, M., Hasani, A., and Kim, S.Y. Novel architecture titanium carbide ($Ti_3C_2T_x$) MXene cocatalysts toward photocatalytic hydrogen production: a mini-review. *Nanomaterials*, 10(4), 602, 2020.

[10] Ghidiu, M., Lukatskaya, M.R., Zhao, M.Q., Gogotsi, Y., and Barsoum, M.W. Conductive two-dimensional titanium carbide 'clay' with high volumetric capacitance. *Nature*, 516(7529): 78-81, 2014.

[11] Li, T., Yao, L., Liu, Q., Gu, J., Luo, R., Li, J., Yan, X., Wang, W., Liu, P., Chen, B., and Zhang, W. Fluorine free synthesis of high purity $Ti_3C_2T_X$ (T= OH, O) via alkali treatment. *Angewandte Chemie*, 57(21): 6115-6119, 2018.

[12] Jawaid, A., Hassan, A., Neher, G., Nepal, D., Pachter, R., Kennedy, W.J., Ramakrishnan, S., and Vaia, R.A. Halogen etch of Ti_3AlC_2 MAX phase for MXene fabrication. *ACS nano*, 15(2): 2771-2777, 2021.

[13] Nandi, S., and Das, S.K. Realizing a low-cost and sustainable rechargeable aqueous aluminum-metal battery with exfoliated graphite cathode. *ACS Sustainable Chemistry & Engineering*, *7*(24): 19839-19847, 2019.

[14] Xiao, Z.L., Han, C.Y., Welp, U., Wang, H.H., Kwok, W.K., Willing, G.A., Hiller, J.M., Cook, R.E., Miller, D.J., and Crabtree, G.W. Fabrication of alumina nanotubes and nanowires by etching porous alumina membranes. *Nano Letters*, *2*(11): 1293-1297, 2002.

[15] Sadeghpour-Motlagh, M., Mokhtari-Zonouzi, K., Aghajani, H., and Kakroudi, M.G. Effects of etching time and NaOH concentration on the production of alumina nanowires using porous anodic alumina template. *Journal of materials engineering and performance*, 23(6): 2007-2014, 2014.

[16] Wang, J., Polleux, J., Lim, J., and Dunn, B. Pseudocapacitive contributions to electrochemical energy storage in TiO_2 (anatase) nanoparticles. *The Journal of Physical Chemistry C*, 111(40): 14925-14931, 2007.

[17] Sarycheva, A., and Gogotsi, Y. Raman spectroscopy analysis of the structure and surface chemistry of $Ti_3C_2T_x$ MXene. *Chemistry of Materials*, 32(8): 3480-3488, 2020.

[18] Krishnamoorthy, K., Pazhamalai, P., Sahoo, S., and Kim, S.J. Titanium carbide sheet based high performance wire type solid state supercapacitors. *Journal of Materials Chemistry A*, 5(12): 5726-5736, 2017.

[19] Parvez, K., Li, R., Puniredd, S.R., Hernandez, Y., Hinkel, F., Wang, S., Feng, X., and Mullen, K. Electrochemically exfoliated graphene as solution-processable, highly conductive electrodes for organic electronics. *ACS nano*, 7(4): 3598-3606, 2013.

[20] Parvez, K., Wu, Z.S., Li, R., Liu, X., Graf, R., Feng, X., and Müllen, K. Exfoliation of graphite into graphene in aqueous solutions of inorganic salts. *Journal of the American Chemical Society*, 136(16): 6083-6091, 2014.